A Family of Highly Accurate Interpolation Functions for Magnitude-Mode Fourier Transform Spectroscopy

C. DALE KEEFE and MELVIN B. COMISAROW*

Department of Chemistry, University of British Columbia, Vancouver, British Columbia V6T 1Y6, Canada

A new family of highly efficient interpolating functions, the *KCe* functions, $KCe(\omega) = (a\omega^2 + b\omega + c)^e$, where *e* is the exponent, is developed for three-point frequency interpolation of discrete, magnitude-mode, apodized Fourier transform spectra. The family is characterized by high interpolation accuracy and ease of implementation. Various members of the family can be generated by varying the exponent. Prior work from this laboratory indicated that the parabola is the interpolating function of choice for interpolation of discrete, apodized magnitude spectra. We show here that, compared to parabolic interpolation, *KCe* interpolation typically gives residual systematic errors which are lower by between one and two orders of magnitude. These systematic errors are analytically derived and the efficacy of interpolation is rigorously examined as a function of the *KCe* exponent, the number of zero-fillings, the amount of damping in the transient, and the window function used to apodize the spectrum. For Hanning-apodized spectra, the *KC*5.5 function gives the lowest residual systematic errors, which are typically 15 times less than those remaining after parabolic interpolation. Similarly, the *KC*6.6 function is optimal for Hamming-apodized spectra (22 times better than parabolic interpolation) and the *KC*9.5 function is optimal for Blackman-Harris-apodized spectra (80 times better than parabolic interpolation). By extrapolation from other optimal *KCe* functions, we estimate that the optimal *KCe* function for interpolation of Kaiser-Bessel-apodized spectra is *KC*12.5. Analytical formulae for propagation of random errors in spectral intensity into random errors in interpolated frequency are derived for parabolic interpolation and for *KCe* interpolation. These error propagation formulae give random errors which are inversely proportional to the SNR of the spectrum. These formulae are evaluated with the appropriate *KCe* exponent for each of the Hanning, the Hamming, and the Blackman-Harris windows. In all cases we find that the random error is essentially independent of both window type and interpolation scheme. While zero-filling prior to interpolation reduces the residual systematic frequency interpolation error, it *increases* the random frequency error. The increase in random error with higher levels of zero-filling is explained. Because the random errors are proportional to noise level, the optimal number of zero-fillings varies with SNR. If the apodizing window is chosen to match the dynamic range of the spectrum, as we have previously recommended, then the systematic error for *KCe* interpolation of non-zero-filled spectra is so low that the overall error is dominated by the random error. In this case, *KCe* interpolation is, for all intents and purposes, exact. Since the random error is minimized by no zero-filling, the lowest overall error will be achieved by a combination of no zero-filling and *KCe* interpolation. In constrast, the minimum total error for parabolic interpolation is achieved by interpolation of the once-zero-filled spectrum. A further advantage of *KCe* interpolation, over and above its lower total error, is that *KCe* interpolation obviates the need for zero-filling.

Index Headings: **Computer applications; Instrumentation, Fourier transform; Mass spectroscopy; Microwave spectroscopy; FT-IR; Spectroscopic techniques.**

INTRODUCTION

Unlike their scanning counterparts, Fourier transform (FT) spectrometers such as FT-nuclear magnetic resonance (FT-NMR), FT-ion cyclotron resonance (FT-ICR), and FT-microwave spectrometers do not give a spectrum directly, but rather generate a transient signal, characteristic of the entire sample. This signal consists of a sum of time-domain signals, each of the form given by Eq. 1,

$$F(t) = 2\pi K \cos(\omega_0 t)\exp(-t/\tau) \qquad 0 < t < T \quad (1)$$

where ω_0 is the resonant frequency, K is a constant proportional to the number of oscillators, τ is the relaxation time of the time-domain signal, and T is the acquisition time of the signal. The amount of damping in the signal is described by the damping ratio T/τ. $T/\tau = 0$ corresponds to an undamped transient; $T/\tau = 3$ characterizes a transient which decays to 5% of its initial value and is essentially completely damped.

The continuous time signal is sampled N times at a sampling rate S

$$T = N/S \quad (2)$$

to give a *discrete* time signal, which is stored. The discrete time signal may be augmented by adding n sets of zeros, with each zero-filling doubling the length of the stored time signal.[1,2] Numerical Fourier transformation of this discrete time signal gives a *discrete* spectrum defined *only* at the discrete frequencies f_m,

$$f_m = \frac{m}{2^n T} \qquad n = 0, 1, 2, \ldots$$
$$m = 0, 1, 2, \ldots, 2^n N - 1 \quad (3)$$

where n is number of zero-fillings and m is the index of the discrete spectrum. The channel spacing, Δf, the frequency distance between two adjacent discrete frequencies, is given by[2]

$$\Delta f = \frac{1}{2^n T} \qquad n = 0, 1, 2, \ldots . \quad (4)$$

Now, the true frequency, $\omega_0/2\pi$ (Eq. 1), will always lie *between* two adjacent frequencies of the discrete spectrum (Eq. 3), and taking the highest local maximum in the discrete spectrum as an experimental measurement of ω_0 will give rise to a systematic error which is inherent in the method (see Fig. 1). This systematic error can be reduced by extended zero-filling, which can reduce the error to less than any desired amount.[2] Zero-filling, though, has the major disadvantage of requiring very large computer memories to store the zero-filled transient and the zero-filled spectrum.

An alternative procedure to minimize the discrete error of experimental Fourier spectra is interpolation.[3,4] In this procedure, a few discrete intensities are used to fit a function from which an interpolated peak location can be calculated. Figure 1 illustrates this approach. Curve

Received 27 September 1989.
* Author to whom correspondence should be sent.

0003-7028/90/4404-0600$2.00/0

C is the continuous magnitude line shape given by Eq. 5.[3,5] Equation 5 gives

$$C_R(\omega) = K\tau\left[1 - 2\exp(-T/\tau)\cos[(\omega - \omega_0)T)] + \exp(-2T/\tau)\right]^{1/2} \cdot \left[\frac{1}{1 + (\omega - \omega_0)^2\tau^2}\right]^{1/2}, \quad (5)$$

the continuous rectangle-apodized magnitude line shape as function of the frequency, ω; the resonant frequency, ω_0; the acquisition time, T; the relaxation time, τ; and the scaling factor, K. Equation 5 is the magnitude Fourier transform, i.e., the modulus of the complex Fourier transform, of Eq. 1. The crosses in Fig. 1 are discrete spectral intensities and are the only points from which to determine the frequency ω_0. Curve KC is an interpolating function derived below. Note that the center frequency, ω_{interp}, of curve KC lies closer to ω_0 than does either of the adjacent frequencies in the discrete spectrum. The residual systematic error of the interpolation method illustrated by Fig. 1 is the difference between ω_{interp} and ω_0.

Two different approaches to interpolation have appeared in the literature. Simple functions, such as the parabola $P(\omega)$, given by Eq. 6,

$$P(\omega) = a\omega^2 + b\omega + c, \quad (6)$$

the Lorentzian function, $L(\omega)$, given by Eq. 7,

$$L(\omega) = \frac{I\tau'}{1 + (\omega - \omega_{interp})^2\tau^2}, \quad (7)$$

and the magnitude-Lorentzian function, $ML(\omega)$, given by Eq. 8,

$$ML(\omega) = K'\left[\frac{\tau'}{1 + (\omega - \omega_{interp})^2\tau^2}\right]^{1/2}, \quad (8)$$

can be used[4,6] to calculate an interpolated frequency, ω_{interp}, which is closer to the true frequency, ω_0, than any of the discrete frequencies, $2\pi f_m$. For interpolating the natural magnitude line shape, Eq. 5, magnitude-Lorentzian interpolation is analytically exact;[3] $\omega_{interp} = \omega_0$. That is, regardless of the value of the damping constant, τ, and regardless of the location of true frequency, ω_0, magnitude-Lorentzian interpolation of the natural magnitude line shape always gives the true frequency ω_0.[3]

The second approach to interpolation involves the derivation and manipulation of the equations needed to *exactly* solve for ω_0. For the non-zero-filled, unapodized, magnitude line shape, this requires interpolation with $ML(\omega)$.[4] $ML(\omega)$ will also exactly interpolate from the non-zero-filled, or once-zero-filled, unapodized, absorption line shape of an undamped transient.[6] In the case of apodized magnitude line shapes, a complicated function can be derived, which, with iterative techniques, will *exactly* solve for the true continuous frequency, ω_0.[7,8]

In the present work, we develop a family of functions, the *KCe* functions, which provide nearly exact interpolation. We examine the residual maximum systematic frequency error remaining after *KCe* interpolation of a discrete, apodized magnitude line shape. The residual

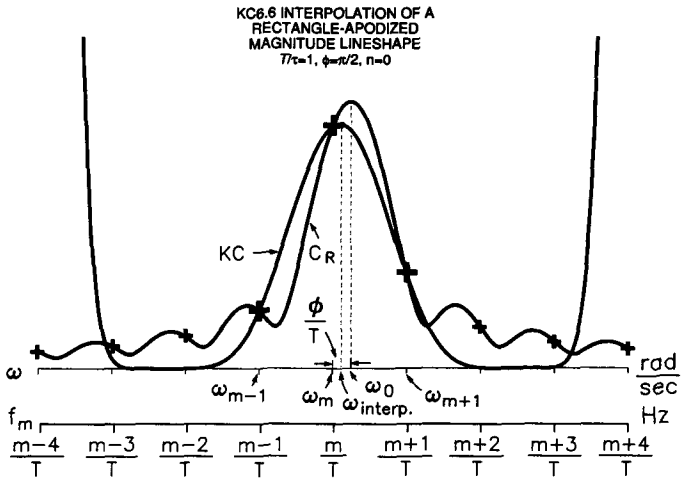

FIG. 1. Rectangle-apodized magnitude line shape and interpolating *KC*6.6 function. Curve C is the continuous magnitude line shape given by Eq. 5, with $T/\tau = 1.0$, which was unapodized before Fourier transformation. The crosses are the values in the non-zero-filled discrete magnitude spectrum for a value of the frequency shift factor $\phi/T = \pi/2$. This value of ϕ/T gives the largest systematic error. The discrete spectrum is defined only at the discrete frequencies given by Eq. 3. m is the index of the discrete spectrum (Eq. 3). Curve KC is the continuous *KC*6.6 function calculated from Eq. 9. The three boldface crosses are the values in the discrete spectrum which were used with Eqs. A1–A3 of the appendix to determine the parameters of curve KC. Note that the frequency of curve KC does not equal that of curve C.

error is examined as a function of the apodizing window, the *KCe* exponent, e (Eq. 9), the damping ratio, T/τ, and the number of zero fillings, n. We find that the optimal *KCe* exponent varies with the window, but that proper selection of the exponent always gives substantial reductions in the residual systematic error. The residual systematic errors can be as much as a factor of 80 lower than the best previously used interpolating functions.

In addition, the simple analytical form of the *KCe* functions allows derivation of formulae for the propagation of *random* errors in spectral amplitude into *random* errors in the interpolated frequency. These random errors *increase* with higher levels of zero-filling. For many cases the *random* error in *KCe* interpolation exceeds the *systematic* error. For these cases, the *KC* interpolation method is, for all intents and purposes, exact. After examining the total interpolation error, the sum of the systematic, and random errors, we conclude that the optimal data treatment procedure is to interpolate the non-zero-filled magnitude spectrum with the appropriate *KCe* function.

RATIONALE FOR THE *KCe* FUNCTIONS

Our prior work[4] on the interpolation of apodized line shapes examined the efficacy with which the parabola, $P(\omega)$, Eq. 6, the Lorentzian function, $L(\omega)$, Eq. 7, and the magnitude-Lorentzian function, $ML(\omega)$, Eq. 8, could interpolate, from the three largest peaks in the discrete spectrum, to an estimation of true frequency, ω_0. Each of these functions can be expressed by the generic formula

$$KCe(\omega) = (a\omega^2 + b\omega + c)^e \quad (9)$$

where a, b, and c are constants chosen to fit the function

to the three discrete intensities and where the exponent e has the value 1 for the parabola, -1 for the Lorentzian, and $-\frac{1}{2}$ for the magnitude-Lorentzian. All three of these values for the exponent, e, gave interpolations which were superior to no interpolation, but with varying efficacies. When examined from this viewpoint, the exponent e in Eq. 9 is a variable which generates a family of interpolating functions of which $P(\omega)$, $L(\omega)$, and $ML(\omega)$ are specific members. It seems reasonable then, that other members of this family could be superior to any of $P(\omega)$, $L(\omega)$, and $ML(\omega)$. It is shown in this work that this is so.

THEORY

Interpolation of Discrete Fourier Spectra. The theoretical framework for the interpolation algorithms follows in part that of our prior work,[3,4] and is repeated here as necessary for completeness. Curve C in Fig. 1 is a *continuous* magnitude line shape and the crosses in Fig. 1 are the values in the *discrete* magnitude spectrum at the discrete frequencies f_m. m is the index of the discrete spectrum. The location, ω_0, of a continuous spectral peak which lies within $\pm\frac{1}{2}\,\Delta f$ of the mth point of the discrete spectrum can be specified in terms of parameters of the discrete spectrum by

$$\omega_0 = \frac{2\pi m + \phi}{2^n T} \tag{10}$$

where the frequency shift angle, ϕ, varies from $-\pi$ (when ω_0 lies halfway between $m-1$ and m) to π (when ω_0 lies halfway between m and $m+1$). The three specific frequencies, ω_{m-1}, ω_m, and ω_{m+1}, in the *continuous* spectrum, which correspond to the three largest values on the spectral peak in the discrete spectrum, are defined in terms of the parameters of the discrete spectrum by

$$\omega_{m-1} = \frac{2\pi(m-1)}{2^n T} \tag{11}$$

$$\omega_m = \frac{2\pi m}{2^n T} \tag{12}$$

$$\omega_{m+1} = \frac{2\pi(m+1)}{2^n T}. \tag{13}$$

The three values in the discrete spectrum which will be used for interpolation are indicated by boldface crosses in Fig. 1.

Quadratic Interpolation. For any second-order polynomial of the form

$$y = ax^2 + bx + c \tag{14}$$

the value x_0 where y is an extremum can be determined[9] from the three pairs of values

$$x_1, y_1; \quad x_2, y_2; \quad x_3, y_3 \tag{15}$$

and the equation

$$x_0 = x_2 - \frac{\Delta x}{2}\left[\frac{y_3 - y_1}{y_1 - 2y_2 + y_3}\right] \tag{16}$$

where Δx is the spacing between equally spaced abscissas, i.e.,

$$\Delta x = x_2 - x_1 = x_3 - x_2. \tag{17}$$

Use of Eq. 16 does not require that the quadratic coefficients a, b, and c be known explicitly. In the following sections various *KCe* functions will be manipulated so that they assume the form of Eq. 14, and Eq. 16 will then be used to calculate an "interpolated peak frequency."

***KCe* Interpolation.** As argued above, a function which could be used for spectral interpolation is the *KCe* function, Eq. 9. *KCe* interpolation is *defined* by the assignment

$$KCe(\omega_m) = C(\omega_m), \qquad m = m-1,\ m,\ m+1 \tag{18}$$

where $C(\omega)$ is *any* magnitude line shape. This interpolation is facilitated by taking the eth root of Eq. 18, which converts the *KCe* function to a quadratic and thus allows use of Eq. 16 for calculating the interpolated frequency, ω_{interp}. Thus, rather than attempt to fit the *KCe* function to the discrete intensities $C(m-1)$, $C(m)$, and $C(m+1)$, we will fit the eth root of the *KCe* function to the eth root of the discrete intensities. Taking these eth roots, making the assignment

$$x_0 = \omega_{\text{interp}} \tag{19}$$

and substituting Eqs. 12, 4, and 18 into Eq. 16 gives Eq. 20:

$$\omega_{\text{interp}} = \frac{2\pi m}{2^n T} - \frac{\pi}{2^n T} \times\left[\frac{(C(\omega_{m+1}))^{1/e} - (C(\omega_{m-1}))^{1/e}}{(C(\omega_{m-1}))^{1/e} - 2(C(\omega_m))^{1/e} + (C(\omega_{m+1}))^{1/e}}\right]. \tag{20}$$

Equation 20 gives ω_{interp}, the interpolated frequency resulting from *KCe* interpolation of the magnitude line shape, as a function of T (Eq. 2), the non-zero-filled acquisition time; n, the number of zero-fillings; e, the *KCe* exponent (Eq. 9); m, the index value of the point in the discrete frequency spectrum which is the discrete local maximum; $C(\omega_m)$, the local maximum; and $C(\omega_{m-1})$ and $C(\omega_{m+1})$, the discrete intensity values on either side of $C(\omega_m)$.

Systematic Errors for KCe Interpolation. Equation 20 gives the interpolated frequency resulting from *KCe* interpolation. The true frequency, i.e., the location of the peak maximum in the continuous spectrum, is ω_0, and thus the systematic error in frequency determination is given by

$$\%\ \text{Error (systematic)} = \frac{\omega_0\ (\text{Eq. } 10) - \omega_{\text{interp}}\ (\text{Eq. } 20)}{\left(\frac{2\pi}{T}\right)} \times 100\%. \tag{21}$$

Equation 21 gives the residual systematic error for three-point *KCe* interpolation of the discrete magnitude line shape as a function of the acquisition time T (Eq. 2). The error is expressed as a percentage of the channel spacing (Eq. 4) in the non-zero-filled discrete spectrum.

Since Eq. 21 depends on Eqs. 10 and 20, which in turn depend upon Eq. 1, Eq. 21 is implicitly a function of K, τ, and ω_0, the parameters of the time-domain signal (Eq. 1), as well as the frequency shift angle, ϕ (Eq. 10), the

number of zero-fillings, n, and the type of apodizing window. Variation of these parameters allows calculation of the systematic interpolation error as a function of all of these variables.

The dependence of the systematic frequency error upon the frequency shift angle, ϕ, merits some discussion. Because the error discussed in this section is systematic and varies from zero when $\phi/T = 0$ to some bounded upper value, we have carried out a methodical search for this upper bound by letting ϕ/T vary over the range $0 < \phi/T < \pi$. Since the line shape is symmetrical, it is unnecessary to search over the range $-\pi < \phi/T < 0$. An increment of $\pi/100$ was used in this search. The error thus found is the *worst-case* error for the particular values of damping ratio, T/τ, and apodizing window used in the search. The calculation was then repeated for different values of the damping ratio T/τ. The maximum residual error, for whatever value of ϕ/T and whatever value of T/τ gave that error, was recorded. The value for the *KCe* exponent e was then incremented by 0.5, and the entire calculation was then repeated for the new value of e. The dependence of the error upon the *KCe* exponent e was noted and, once an error minimum was found, a fine search in increments of $\Delta e = 0.1$ was conducted to find a superior value of e. The second through fourth columns of Table I give the absolute value of maximum interpolation error, for whatever value of T/τ and whatever value of ϕ gave that error, as a function of the *KCe* exponent. The boldface numbers in the first column of Table I give the value of e which gave the lowest error. The boldface numbers in each of the other columns give the corresponding lowest error for the indicated window.

All of the above calculations were then repeated for zero-filled spectra. However, the optimal value of the *KCe* exponent e was virtually the same as the optimal value for no zero-filling ($n = 0$) given in Table I.

Random Errors for KCe Interpolation. Equations 20 and 21 give the *systematic* error in frequency determination which remains after three-point *KCe* interpolation of a magnitude line shape. This systematic error derives from a limitation of the experimental method, namely the discrete nature of the experimental Fourier spectrum. In addition to this systematic error there is also a *random* error in the interpolated frequency. These random *frequency* errors derive from random *amplitude* errors in the discrete magnitude intensities, $C(\omega_m)$, $m = m - 1, m, m + 1$. By use of standard error propagation formulae,[10] analytical formulae for the random frequency error, $\Delta\omega$, can be derived as functions of the random amplitude error. This random frequency error is given by Eq. 22 (see below), where

$$X_i = [C(\omega_i)]^{1/e} \qquad i = m - 1, m, m + 1 \quad (23)$$

and

$$\Delta X_i = \frac{1}{e}[C(\omega_i)]^{1/e-1}\Delta C \qquad i = m - 1, m, m + 1 \quad (24)$$

TABLE I. Maximum residual systematic frequency error (T/τ = (0-3.0)[a] for interpolation of non-zero-filled, apodized, magnitude line shapes as function of *KCe* exponent, *e*.

KCe exponent, e[b]	Hanning interpolation error (%)	Hamming interpolation error (%)	Blackman-Harris interpolation error (%)
2.5	1.660	2.149	2.005
3.0	1.259	1.654	1.170
3.5	0.970	1.299	0.934
4.0	0.754	1.033	0.757
4.5	0.586	0.826	0.620
5.0	0.452	0.661	0.509
5.3	0.383	—	—
5.4	0.362	—	—
5.5	**0.342**	0.525	0.419
5.6	0.360	—	—
5.7	0.382	—	—
6.0	0.443	0.412	0.344
6.4	—	0.334	—
6.5	0.532	0.317	0.280
6.6	—	**0.306**	—
6.7	—	0.325	—
6.8	—	0.344	—
7.0	0.608	0.380	0.226
7.5	0.674	0.461	0.179
8.0	0.732	0.532	0.137
8.5	0.783	0.595	0.101
9.0	0.828	0.651	0.068
9.3	—	—	0.051
9.4	—	—	0.045
9.5	0.869	0.701	**0.041**
9.6	—	—	0.046
9.7	—	—	0.052
10.0	0.906	0.746	0.068

[a] Maximum systematic frequency error, calculated from Eq. 21, for whatever value of T/τ and whatever value of ϕ that gave the largest error, expressed as a percentage of the channel spacing (Eq. 4) in the non-zero-filled discrete spectrum. The optimal value of e for each window and the corresponding error are in boldface. The optimal values for zero-filled spectra (n = 1–3) were also calculated. In all cases, the optimal values of e increased very slightly, but agreed with those given above within ±0.4.

[b] Equation 9.

and ΔC is the amplitude noise at each point in the discrete spectrum. For use in Eq. 22, we have set ΔC to be a given fraction of the *continuous* peak height, $C(\omega_0)$.

Equations 22–24 give $\Delta\omega$, the random error in the *KCe* interpolated frequency resulting from propagation through Eq. 20 of ΔC, the random error in intensity, as a function of the acquisition time, T (Eq. 2), the discrete magnitude intensities, $C(\omega_m)$, $m = m - 1, m, m + 1$, and the random error in amplitude, ΔC. The error is expressed as a fraction of the channel spacing in the non-zero-filled discrete spectrum. Equation 22 is valid for any *KCe* function, for any magnitude line shape, for any value of the frequency shift angle ϕ, for any number of zero-fillings, n, and for any value of any of the parameters of Eq. 1.

Because the random error in frequency is a function of ϕ (Eq. 10) and since all values of ϕ are equally probable, we have calculated the average value of the random error

$$\Delta\omega = \frac{\dfrac{\pi(X_{m+1} - X_{m-1})}{2^n T(X_{m-1} - 2X_m + X_{m+1})}\left(\dfrac{\Delta X_{m+1}^2 + \Delta X_{m-1}^2}{(X_{m+1} - X_{m-1})^2} + \dfrac{\Delta X_{m-1}^2 + 4\Delta X_m^2 + \Delta X_{m+1}^2}{(X_{m-1} - 2X_m + X_{m+1})^2}\right)^{1/2}}{2\pi/T} \quad (22)$$

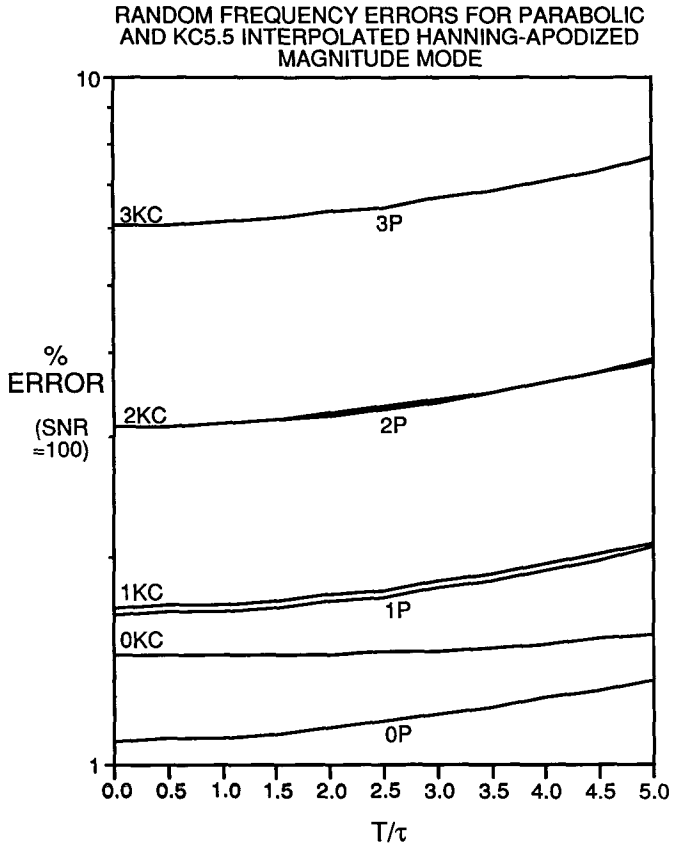

FIG. 2. Random frequency errors for parabolic (P curves) and $KC5.5$ (KC curves) interpolation of the zero-filled, Hanning-apodized, magnitude line shape as a function of T/τ.The errors are expressed as a percentage of the channel spacing in the non-zero-filled discrete spectrum (Eq. 3). The curves give the average random frequency error remaining after interpolation of the Hanning-apodized, zero-filled, discrete line shape for which the noise level is 1% of the peak maximum (SNR = 100). For example, curve $2KC$ gives the average frequency error remaining after $KC5.5$ interpolation of the Hanning-apodized, twice-zero-filled, discrete magnitude spectrum. Curve $0P$ gives the average frequency error remaining after parabolic interpolation of the Hanning-apodized, non-zero-filled, discrete magnitude spectrum. These error curves were calculated from Eqs. 22 and 36, with $e = 1$ for the P curves and $e = 5.5$ for the KC curves and then averaged according to Eqs. 25 and 26, as described in the text. The errors in this figure arise from the finite signal-to-noise ratio of the experimental data and should be added to the systematic errors given in Fig. 3 to predict the total error for a given experimental situation. The errors in this figure are proportional to the noise level (Eq. 24) and would be 10 times less for an SNR of 1000, 10 times greater for an SNR of 10, etc.

by averaging the random error over the range $0 < \phi < \pi$.

$$\Delta\omega_{avr} = \frac{1}{\pi}\int_0^{\pi} \Delta\omega \text{ (Eq. 22) } d\phi \qquad (25)$$

$$\%\text{ Error (random)} = \Delta\omega_{avr} \text{ (Eq. 25)} \times 100\%. \qquad (26)$$

Because the line shape is symmetrical, it is unnecessary to average over the range $-\pi < \phi < \pi$. Equation 26 gives the average random error in frequency after KCe interpolation. The error is expressed as a percentage of the channel spacing (Eq. 4) in the non-zero-filled spectrum. In this work, the integral in Eq. 25 was evaluated numerically with the use of an increment $\Delta\phi = \pi/100$. The *random* errors were only calculated for the optimal values of e, i.e., the values of e which gave the lowest *systematic* errors, as described above.

Preceding sections lay the theoretical framework for KCe interpolation, and for deriving the associated systematic and random errors. The following sections describe the application of this framework to specific apodized line shapes.

OPTIMAL *KCe* FUNCTION FOR INTERPOLATION OF HANNING-APODIZED MAGNITUDE SPECTRA

The Hanning Window and the Hanning-Apodized Line Shape. The Hanning window is suitable for spectra with dynamic ranges of up to 30:1.[11] The Hanning window, $\mathrm{Hn}(t)$, is defined by Eq. 27:[12]

$$\mathrm{Hn}(t) = \sin^2(\pi t/T) = [1 - \cos(2\pi t/T)]/2, \quad 0 < t < T. \qquad (27)$$

The analytical magnitude spectrum, $C_{\mathrm{Hn}}(\omega)$, the modulus of the complex Fourier tranform, of the time-domain signal, which was windowed with the Hanning window (Eq. 27), prior to Fourier transformation, is given by Eq. 28:

$$C_{\mathrm{Hn}}(\omega) = K\tau\left[1 - 2\exp(-T/\tau)\cos[(\omega - \omega_0)T] + \exp(-2T/\tau)\right]^{1/2} \times \left[\frac{4\pi^4\tau^4}{A_0 + A_1\omega + A_2\omega^2 + A_3\omega^3 + A_4\omega^4 + A_5\omega^5 + A_6\omega^6}\right]^{1/2} \qquad (28)$$

where:

$$A_0 = \tau^6T^4\omega_0^6 - 8\tau^6T^2\pi^2\omega_0^4 + 3\tau^4T^4\omega_0^4 + 16\tau^6\pi^4\omega_0^2 + 3\tau^2T^4\omega_0^2 + 16\tau^4\pi^4 + 8\tau^2T^2\pi^2 + T^4 \qquad (29)$$

$$A_1 = -6\tau^6T^4\omega_0^5 + 32\tau^6T^2\pi^2\omega_0^3 - 12\tau^4T^4\omega_0^3 - 32\tau^6\pi^4\omega_0 - 6\tau^2T^4\omega_0 \qquad (30)$$

$$A_2 = 15\tau^6T^4\omega_0^4 - 48\tau^6T^2\pi^2\omega_0^2 + 18\tau^4T^4\omega_0^2 + 16\tau^6\pi^4 + 3\tau^2T^4 \qquad (31)$$

$$A_3 = -20\tau^6T^4\omega_0^3 + 32\tau^6T^2\pi^2\omega_0 - 12\tau^4T^4\omega_0 \qquad (32)$$

$$A_4 = 15\tau^6T^4\omega_0^2 - 8\tau^6T^2\pi^2 + 3\tau^4T^4 \qquad (33)$$

$$A_5 = -6\tau^6T^4\omega_0 \qquad (34)$$

$$A_6 = \tau^6T^4. \qquad (35)$$

Equation 28 gives the continuous, Hanning-apodized, magnitude line shape as a function of the parameters of Eq. 1. It is taken from the literature.[7]

Systematic Errors for *KCe* Interpolation of the Hanning Line Shape. The systematic errors for the Hanning line shape can be calculated by substituting Eq. 36 into Eq. 20.

$$C(\omega_m) = C_{\mathrm{Hn}}(\omega_m) \text{ (Eq. 28)}, \quad m = m - 1, m, m + 1. \qquad (36)$$

The above procedure was used to find the optimal value of the KCe exponent e for the Hanning-apodized line shape. The results of a coarse and a fine search for the optimal value of e are given in the second column of Table I. The optimal value of the KCe exponent for KCe interpolation of Hanning-apodized line shapes is 5.5. Figure 2 shows the analytically calculated, residual worst-case systematic errors, for whatever value of ϕ (Eq. 10)

that gave that error, as a function of the damping ratio, T/τ, for $KC5.5$ interpolation of a zero-filled, Hanning-apodized magnitude spectrum and the corresponding calculated worst-case errors for parabolic interpolation ($e = 1$). Note that the $KC5.5$ errors are lower than the parabolic errors by about a factor of 15. Note further that, for both $KC5.5$ interpolation and parabolic interpolation, the residual systematic errors are lowered by about an order of magnitude for each additional level of zero-filling.

The random error for $KC5.5$ interpolation of the non-zero-filled Hanning line shape for a signal-to-noise ratio (SNR) of 30:1 is indicated in Fig. 3. This error is derived from the $0KC$ data of Fig. 2. The maximum SNR for which the Hanning window is suitable is 30:1.[11] This error is inversely proportional to SNR and will be greater for lower SNRs. Note that the random error in the graph is greater than the systematic error.

Random Errors for *KCe* Interpolation of the Hanning Line Shape. The random error was calculated from Eq. 26 by substituting Eq. 36 into Eqs. 22–24. The results are graphically displayed in Fig. 2. Figure 2 shows the analytically calculated, average random errors as a function of the damping ratio, T/τ, for $KC5.5$ interpolation of a zero-filled, Hanning-apodized magnitude spectrum and the corresponding average errors for parabolic interpolation ($e = 1$). These errors are inversely proportional to the presumed SNR and are shown in Fig. 2 for an SNR = 100. The errors are expressed as a percentage of the non-zero-filled channel spacing. Note that the $KC5.5$ errors are about the same as the parabolic errors except for no zero-filling, where the $KC5.5$ errors are slightly greater. Unlike the systematic errors shown in Fig. 3, the random errors in Fig. 2 are essentially independent of the interpolating function. Note that for both $KC5.5$ interpolation and for parabolic interpolation, more zero-filling *increases* the random error.

The lowest random error for KCe interpolation is for the no zero-filling case. Figure 2 was derived for SNR = 100:1 for easy comparison with Figs. 5 and 8. Since the Hanning window should only be used if SNR < 30:1,[11] we have indicated the random error for the optimal case ($0KC$) for SNR = 30:1 in Fig. 3.

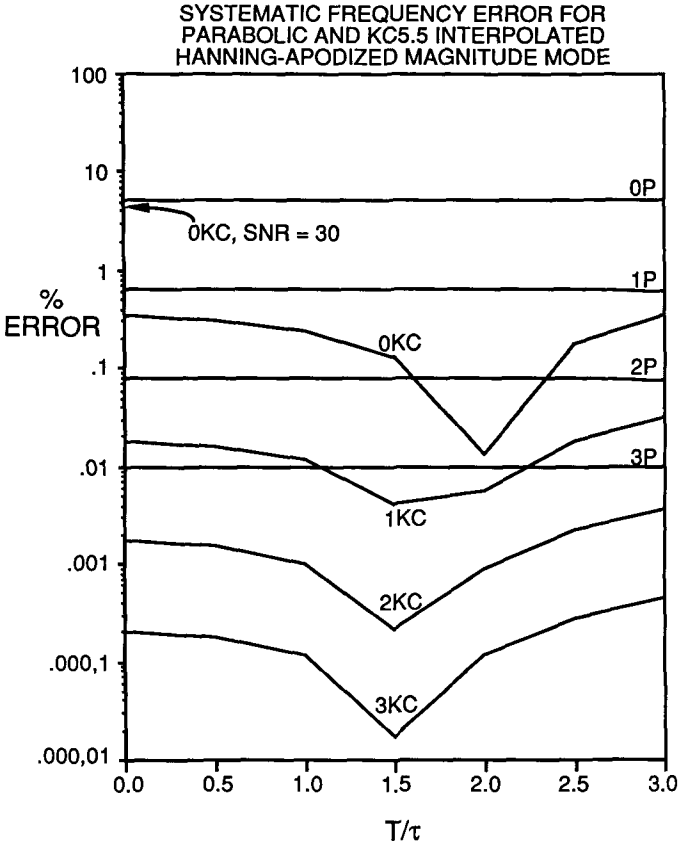

FIG. 3. Systematic frequency errors for parabolic (P curves) and $KC5.5$ (KC curves) interpolation of the zero-filled, Hanning-apodized, magnitude line shape as a function of T/τ. The errors are expressed as a percentage of the channel spacing in the non-zero-filled discrete spectrum (Eq. 3). The curves give the maximum frequency error remaining after interpolation of the Hanning-apodized, zero-filled discrete line shape. For example, curve $2KC$ gives the maximum frequency error remaining after $KC5.5$ interpolation of the Hanning-apodized, twice-zero-filled, discrete magnitude spectrum. Curve $0P$ gives the maximum frequency error remaining after parabolic interpolation of the Hanning-apodized, non-zero-filled, discrete magnitude spectrum. These error curves were calculated from the absolute values of Eqs. 21 and 36, with $e = 1$ for the P curves and $e = 5.5$ for the KC curves. The errors in this figure presume an infinite signal-to-noise ratio and should be added to the random errors given in Fig. 3 to predict the total error for a given experimental situation. The arrow indicates the random error, derived from the $0KC$ data in Fig. 2, for SNR = 30.

OPTIMAL *KCe* FUNCTION FOR INTERPOLATION OF HAMMING-APODIZED MAGNITUDE SPECTRA

The Hamming Window and the Hamming-Apodized Line Shape. The Hamming window has been recommended as suitable for spectra with dynamic ranges of up to 100:1.[11] The Hamming window, $\mathrm{Hm}(t)$, is defined by Eq. 37:[12]

$$\mathrm{Hm}(t) = 0.54 - 0.46\cos(2\pi t/T), \qquad 0 < t < T. \tag{37}$$

The analytical magnitude spectrum, $C_{\mathrm{Hm}}(\omega)$, the modulus of the complex Fourier transform, of the time-domain signal (Eq. 1), which was windowed with the Hamming window (Eq. 37), prior to Fourier transformation, is given by Eq. 38 (see below).

$$C_{\mathrm{Hm}}(\omega) = K\tau\left[1 - 2\exp(-T/\tau)\cos[(\omega-\omega_0)T] + \exp(-2T/\tau)\right]^{1/2} \times\left[\frac{(0.54)^2}{1+(\omega-\omega_0)^2\tau^2} - \frac{2(0.54)(0.46)\left[1+\tau^2[(\omega-\omega_0)^2+4\pi^2/T^2]+(\omega-\omega_0)^2\tau^2[1+\tau^2((\omega-\omega_0)^2-4\pi^2/T^2)]\right]}{\left[[1+(\omega-\omega_0)^2\tau^2]\{1+2\tau^2[(\omega-\omega_0)^2+4\pi^2/T^2]+\tau^4[(\omega-\omega_0)^2-4\pi^2/T^2]^2\}\right]} + \frac{(0.46)^2[(1+\tau^2((\omega-\omega_0)^2+4\pi^2/T^2))^2+(\omega-\omega_0)^2\tau^2(1+\tau^2((\omega-\omega_0)^2-4\pi^2/T^2))^2]}{\left[1+2\tau^2[(\omega-\omega_0)^2+4\pi^2/T^2]+\tau^4[(\omega-\omega_0)^2-4\pi^2/T^2]^2\right]^2}\Bigg]^{1/2} \tag{38}$$

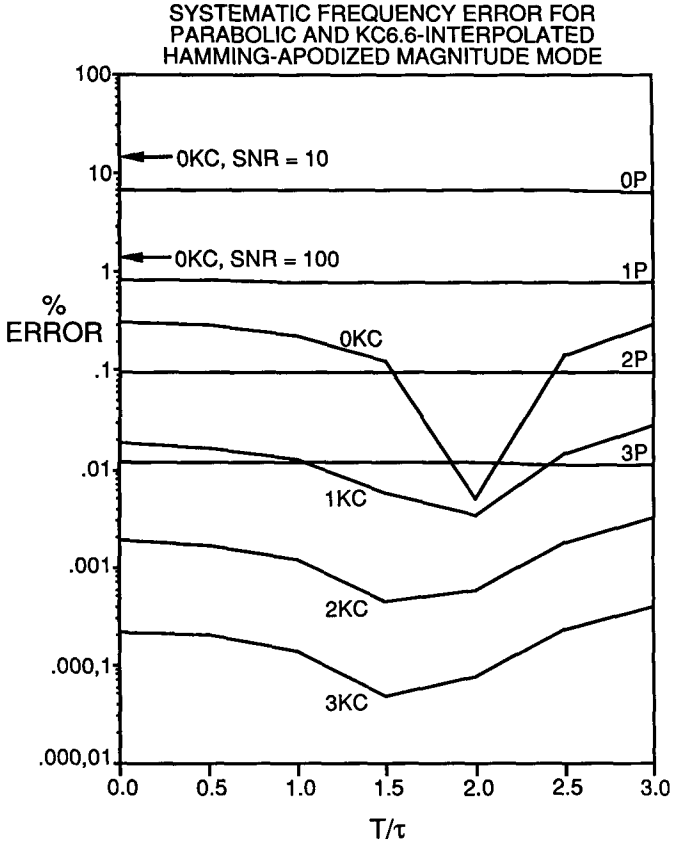

FIG. 4. Systematic frequency errors for parabolic (P curves) and $KC6.6$ (KC curves) interpolation of the zero-filled, Hamming-apodized magnitude line shape as a function of T/τ. The errors are expressed as a percentage of the channel spacing in the non-zero-filled discrete spectrum (Eq. 3). The curves give the maximum frequency error remaining after interpolation of the Hamming-apodized, zero-filled discrete line shape. For example, curve $2KC$ gives the maximum frequency error remaining after $KC6.6$ interpolation of the Hamming-apodized, twice-zero-filled, discrete magnitude spectrum. Curve $0P$ gives the maximum frequency error remaining after parabolic interpolation of the Hamming-apodized, non-zero-filled, discrete magnitude spectrum. These error curves were calculated from the absolute values of Eqs. 21 and 39 with $e = 1$ for the P curves and $e = 6.6$ for the KC curves. The errors in this figure presume an infinite signal-to-noise ratio and should be added to the random errors given in Fig. 5 to predict the total error for a given experimental situation. The arrows indicate the random error, derived from the $0KC$ data in Fig. 5, for SNR = 10 and SNR = 100.

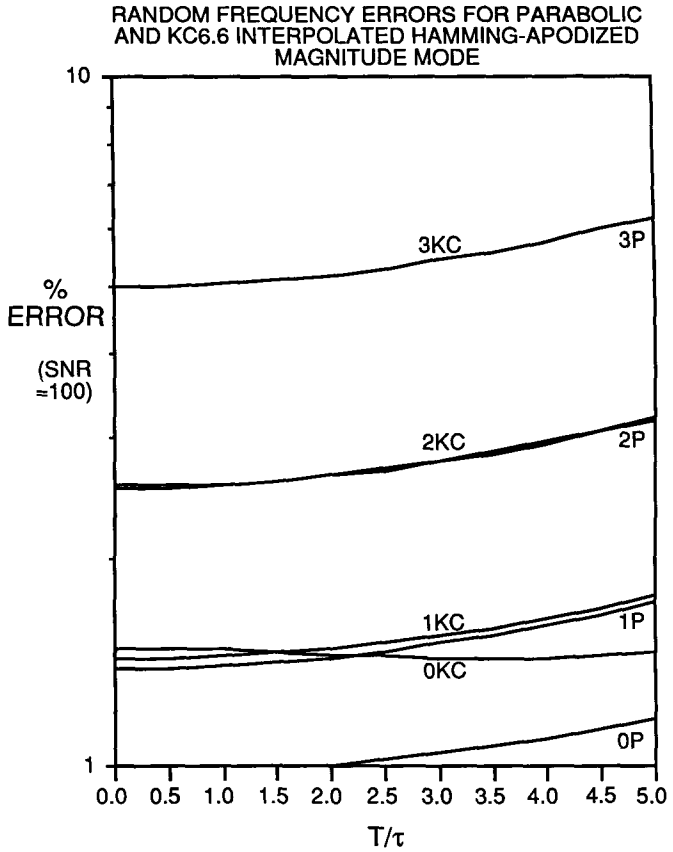

FIG. 5. Random frequency errors for parabolic (P curves) and $KC6.6$ (KC curves) interpolation of the zero-filled, Hamming-apodized magnitude line shape as a function of T/τ. The errors are expressed as a percentage of the channel spacing in the non-zero-filled discrete spectrum (Eq. 3). The curves give the average random frequency error remaining after interpolation of the Hamming-apodized, zero-filled, discrete line shape for which the noise level is 1% of the peak maximum (SNR = 100). For example, curve $2KC$ gives the average frequency error remaining after $KC6.6$ interpolation of the Hamming-apodized, twice-zero-filled, discrete magnitude spectrum. Curve $0P$ gives the average frequency error remaining after parabolic interpolation of the Hamming-apodized, non-zero-filled, discrete magnitude spectrum. These error curves were calculated from Eqs. 22 and 39 with $e = 1$ for the P curves and $e = 6.6$ for the KC curves and then averaged according to Eqs. 25 and 26 as described in the text. The errors in this figure arise from the finite signal-to-noise ratio of the experimental data and should be added to the systematic errors given in Fig. 4 to predict the total error for a given experimental situation. The errors in this figure are proportional to the noise level (Eq. 24) and would be 10 times less for an SNR of 1000, 10 times greater for an SNR of 10, etc.

Equation 38 gives the continuous Hamming-apodized magnitude line shape as function of the parameters of Eq. 1. It is presented here for the first time.

Systematic Errors for *KCe* Interpolation of the Hamming Line Shape. The above procedure was used to find the optimal value of the KCe exponent e for the Hamming-apodized line shape by substituting Eq. 39 into Eq. 20. The results of a coarse and a fine search

$$C(\omega_m) = C_{Hm}(\omega_m) \text{ (Eq. 38)}, \quad m = m - 1, m, m + 1, \tag{39}$$

for the optimal value of e are given in the third column of Table I. The optimal value of the KCe exponent for KCe interpolation of Hamming-apodized line shapes is 6.6. Figure 4 shows the analytically calculated, residual worst-case systematic errors as a function of the damping ratio, T/τ, for $KC6.6$ interpolation of a zero-filled, Hamming-apodized magnitude spectrum and the corresponding worst-case errors for parabolic interpolation ($e = 1$). The parabolic errors were previously derived[4] by numerical techniques. Note that the $KC6.6$ errors are lower than the parabolic errors by about a factor of 40. Note further that the residual systematic errors are lowered by about an order of magnitude for each additional level of zero-filling.

The random errors for $KC6.6$ interpolation of the non-zero-filled Hamming line shape for SNRs of 10 and 100 are indicated in Fig. 4. These errors are taken from the $0KC$ data of Fig. 5. Note that the random errors are greater than the systematic error.

Random Errors for *KCe* Interpolation of the Hamming Line Shape. The random error was calculated from Eq. 26 by substituting Eq. 39 into Eqs. 22–24. The results are graphically displayed in Fig. 5. Figure 5 shows the analytically calculated, average random errors as a func-

tion of the damping ratio, T/τ, for $KC6.6$ interpolation of a zero-filled, Hamming-apodized magnitude spectrum and the corresponding average errors for parabolic interpolation ($e = 1$). These errors are inversely proportional to the presumed SNR and are shown in Fig. 5 for SNR = 100:1. The errors are expressed as a percentage of the non-zero-filled channel spacing. Note that the $KC6.6$ errors are about the same as the parabolic errors except for no zero-filling, for which the $KC6.6$ errors are slightly greater. Unlike the systematic errors shown in Fig. 4, the random errors in Fig. 5 are essentially independent of the interpolating function. Note that, for both $KC6.6$ interpolation and for parabolic interpolation, more zero-filling *increases* the random error.

The lowest random error for KCe interpolation is for the no zero-filling case. Figure 5 was derived for SNR = 100:1, which is the same SNR used for Figs. 3 and 8. Since the Hamming window is suitable for spectra with dynamic ranges of up to 100:1, the random errors for no zero-filling ($0KC$) and SNR = 100 and 10 are also indicated in Fig. 4.

OPTIMAL *KCe* FUNCTION FOR INTERPOLATION OF BLACKMAN-HARRIS-APODIZED MAGNITUDE SPECTRA

The Blackman-Harris Window and the Blackman-Harris-Apodized Line Shape. The Blackman-Harris window has been recommended as suitable for dynamic ranges of 100:1 to 1000:1[11] The Blackman-Harris window, BH(t), is defined by Eq. 40.[12]

$$\mathrm{BH}(t) = 0.42323 - 0.49755\cos(2\pi t/T) + 0.07922\cos(4\pi t/T), \quad 0 < t < T. \tag{40}$$

The analytical magnitude spectrum, $C_{\mathrm{BH}}(\omega)$, the modulus of the complex Fourier transform, of the time-domain signal (Eq. 1), which was windowed with the Blackman-Harris window (Eq. 40), prior to Fourier transformation, is given by Eq. 41 (see below), where:

$$A_1 = \tau^2((\omega - \omega_0)^2 + 4\pi^2/T^2) \tag{42}$$
$$A_2 = \tau^2((\omega - \omega_0)^2 - 4\pi^2/T^2) \tag{43}$$
$$A_3 = \tau^2((\omega - \omega_0)^2 + 16\pi^2/T^2) \tag{44}$$
$$A_4 = \tau^2((\omega - \omega_0)^2 - 16\pi^2/T^2). \tag{45}$$

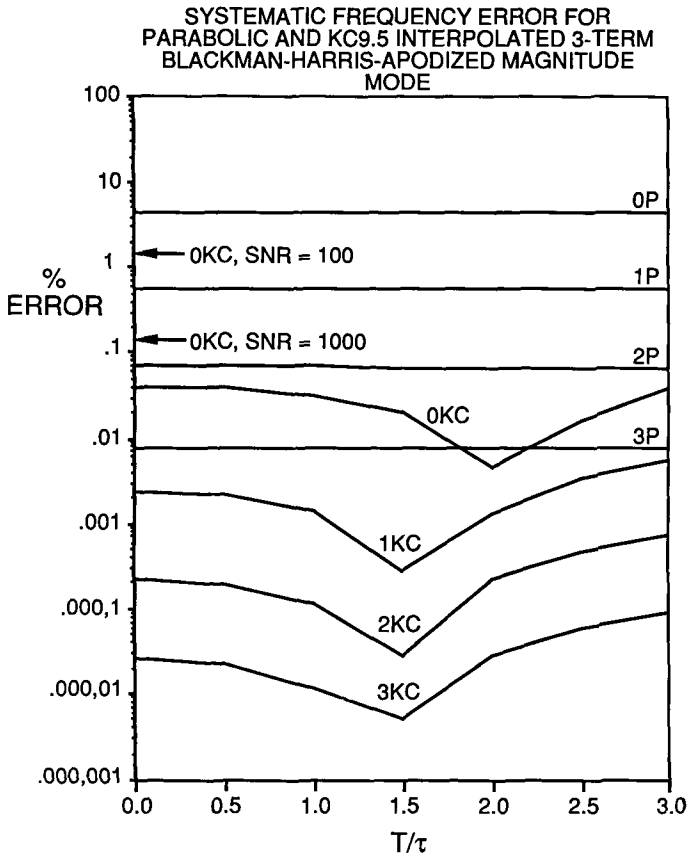

FIG. 6. Systematic frequency errors for parabolic (P curves) and $KC9.5$ (KC curves) interpolation of the zero-filled, Blackman-Harris-apodized, magnitude line shape as a function of T/τ. The errors are expressed as a percentage of the channel spacing in the non-zero-filled discrete spectrum (Eq. 3). The curves give the maximum frequency error remaining after interpolation of the Blackman-Harris-apodized, zero-filled discrete line shape. For example, curve $2KC$ gives the maximum frequency error remaining after $KC9.5$ interpolation of the Blackman-Harris-apodized, twice-zero-filled, discrete magnitude spectrum. Curve $0P$ gives the maximum frequency error remaining after parabolic interpolation of the Blackman-Harris-apodized, non-zero-filled, discrete magnitude spectrum. These error curves were calculated from the absolute values of Eqs. 21 and 46 with $e = 1$ for the P curves and $e = 9.5$ for the KC curves. The errors in this figure presume an infinite signal-to-noise ratio and should be added to the random errors given in Fig. 8 to predict the total error for a given experimental situation. The arrows indicate the random error, derived from the $0KC$ data in Fig. 8 for SNR = 100 and SNR = 1000.

$$\begin{aligned} C_{\mathrm{BH}}(\omega) = K\tau\Big[1 - 2\exp(-T/\tau)\cos[(\omega - \omega_0)T] + \exp(-2T/\tau)\Big]^{1/2} \\ \times\Bigg[\frac{(0.42323)^2}{1 + (\omega - \omega_0)^2\tau^2} + \frac{(0.49755)^2[(1 + A_1)^2 + (\omega - \omega_0)^2\tau^2(1 + A_2)^2]}{(1 + 2A_1 + A_2^2)^2} \\ + \frac{(0.07922)^2[(1 + A_3)^2 + (\omega - \omega_0)^2\tau^2(1 + A_4)^2]}{(1 + 2A_3 + A_4^2)^2} \\ - \frac{2(0.49755)(0.42323)[1 + A_1 + (\omega - \omega_0)^2\tau^2(1 + A_2)]}{(1 + (\omega - \omega_0)^2\tau^2)(1 + 2A_1 + A_2^2)} \\ + \frac{2(0.07922)(0.42323)[(1 + A_3 + (\omega - \omega_0)^2\tau^2(1 + A_4)]}{(1 + (\omega - \omega_0)^2\tau^2)(1 + 2A_3 + A_4^2)} \\ - \frac{2(0.07922)(0.49755)[(1 + A_3)(1 + A_1) + (\omega - \omega_0)^2\tau^2(1 + A_4)(1 + A_2)]}{[1 + 2A_3 + A_4^2][1 + 2A_1 + A_2^2]}\Bigg]^{1/2} \end{aligned} \tag{41}$$

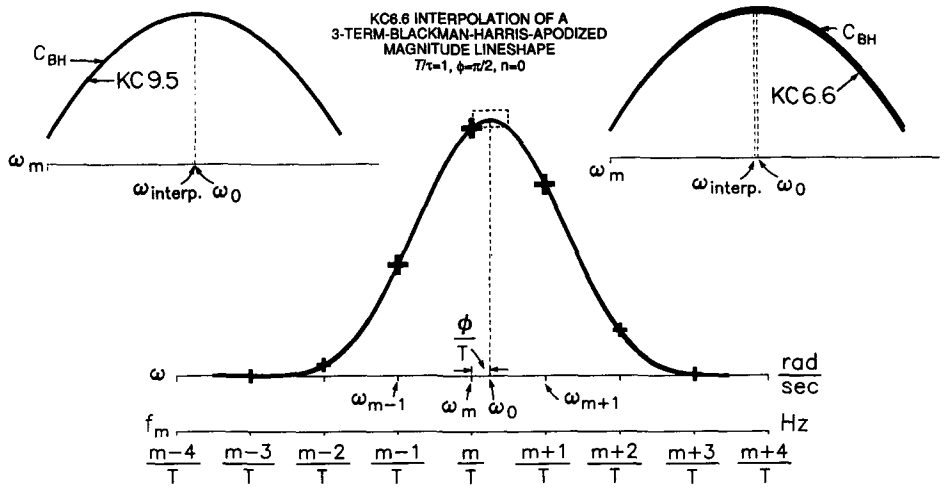

FIG. 7. Three-term-Blackman-Harris-apodized magnitude line shape and interpolating *KC*6.6 function. The *KC*6.6 function is the optimal *KCe* function for interpolation of the Hamming line shape. Curve *C* is the continuous magnitude line shape given by Eq. 41, with $T/\tau = 1.0$. The crosses are the values in the non-zero-filled discrete magnitude spectrum for a value of the frequency shift factor $\phi/T = \pi/2$. This value of ϕ/T gives the largest systematic error. The discrete spectrum is only defined at the discrete frequencies given by Eq. 3. *m* is the index of the discrete spectrum (Eq. 3). Curve *KC*6.6 is the continuous *KC*6.6 function calculated from Eq. 9. The three boldface crosses are the values in the discrete spectrum which were used with Eqs. A1–A3 of the appendix to determine the parameters of curve *KC*6.6. Note that over the region from m − 3 to m + 3, curve *KC*6.6 is virtually a perfect fit to curve C_{BH}. The right-hand inset shows the *KC*6.6 function and the continuous magnitude Blackman-Harris line shape, C_{BH}, over the small region from ω_m to $\omega_{m+0.5}$, indicated by a dotted rectangle at the top of the main figure. The scale in this inset, both horizontally and vertically, is expanded by a factor of ten. Note the very slight mismatch between C_{BH} and *KC*6.6. The left inset was created like the right inset, but for the *KC*9.5 function. *KC*9.5 is the optimal *KCe* function for interpolation of the Blackman-Harris line shape (Table I). Within the scale and penwidth limits of the left inset, the *KC*9.5 function is *indistinguishable* from C_{BH}.

Equation 41 gives the continuous Blackman-Harris-apodized magnitude line shape as function of the parameters of Eq. 1. It is presented here for the first time.

Systematic Errors for *KCe* Interpolation of the Blackman-Harris Line Shape. The above procedure was used to find the optimal value of the *KCe* exponent *e* for the Blackman-Harris-apodized line shape by substituting Eq. 46 into Eq. 20. The results of a coarse and a fine search

$$C(\omega_m) = C_{BH}(\omega_m) \text{ (Eq. 41)}, \quad m = m - 1,\ m,\ m + 1, \tag{46}$$

for the optimal value of *e* are given in the fourth column of Table I. The optimal value of the *KCe* exponent for *KCe* interpolation of Blackman-Harris-apodized line shapes is 9.5. Figure 6 shows the analytically calculated, residual worst-case systematic errors as function of the damping ratio, T/τ, for *KC*9.5 interpolation of a zero-filled Blackman-Harris-apodized magnitude spectrum and the corresponding worst-case errors for parabolic interpolation ($e = 1$). The parabolic errors were previously derived[4] by numerical techniques. Note that the *KC*9.5 errors are lower than the parabolic errors by about a factor of 80. Note further that the residual systematic errors are lowered by about an order of magnitude for each additional level of zero-filling.

The random errors for *KC*9.5 interpolation of the non-zero-filled Blackman-Harris line shape, for SNRs of 100 and 1000, are indicated in Fig. 6. These errors are taken from the 0*KC* data of Fig. 5. Note that the random errors are greater than the systematic error for both cases.

Figure 7 graphically displays the efficacy of *KCe* interpolation, even for nonoptimal *KCe* functions. Figure 7 shows a Blackman-Harris-apodized line shape, C_{BH}, calculated from Eq. 41 with $T/\tau = 1.0$. The crosses in the figure are the discrete magnitude values in the non-zero-filled discrete spectrum for ϕ/T (Eq. 10) $= \pi/2$. The three boldface crosses are the three largest intensities on the line shape in the discrete spectrum. Also displayed in the figure is the *KC*6.6 function calculated from the three discrete largest intensities via Eqs. A1–A2 of the appendix. Note that, even though the *KC*9.5 is the optimal *KCe* interpolating function for C_{BH} (Table I and Fig. 6), the *KC*6.6 function is a remarkably good mimic for the line shape. The right inset of the figure shows the boxed region at the peak maximum, expanded by a factor of 10. Note the very slight mismatch between C_{BH} and *KC*6.6, which is evident at this expanded scale. The left inset shows the same expanded region but for a fitted *KC*9.5 function. *KC*9.5 is the optimal *KCe* function for the C_{BH}. Even on this expanded scale, *KC*9.5 and C_{BH} are indistinguishable.

Random Errors for *KCe* Interpolation of the Blackman-Harris Line Shape. The random error was calculated from Eq. 26 by substituting Eq. 46 into Eqs. 22–24. The results are graphically displayed in Fig. 8. Figure 8 shows the analytically calculated, average random errors as function of the damping ratio, T/τ, for *KC*9.5 interpolation of a zero-filled, Blackman-Harris-apodized magnitude spectrum and the corresponding calculated average errors for parabolic interpolation ($e = 1$). These errors are inversely proportional to the presumed SNR and are shown in Fig. 8 for SNR = 100. The errors are expressed as a percentage of the non-zero-filled channel spacing. Note that the *KC*9.5 errors are about the same as the parabolic errors except for no zero-filling, where the *KC*9.5 errors are slightly greater. Unlike the systematic errors shown in Fig. 6, the random errors in Fig. 8 are essentially independent of the interpolating function. Note that, for both *KC*9.5 interpolation and for parabolic interpolation, more zero-filling *increases* the random error.

The lowest random error for *KCe* interpolation of the Blackman-Harris line shape is for the no zero-filling case. Figure 8 was derived for SNR = 100:1, which is the same SNR used for Figs. 3 and 5. Since the Blackman-Harris window is suitable for spectra with dynamic ranges spanning 100:1 to 1000:1,[11] the random errors for 0*KC* interpolation for SNR = 100 and SNR = 1000 are also indicated on Fig. 6.

DISCUSSION

Choice of Window and Dynamic Range of the Spectrum. The "natural" magnitude line shape, Eq. 5, which is the magnitude Fourier transform of Eq. 1, is notorious for its broad skirt of intensity, which extends for many line widths away from the peak center.[11-13] This skirt exists both for undamped and heavily damped time signals.[11,13] The broad skirt of one peak overlaps nearby peaks and can even obscure nearby small peaks. The skirt can be minimized by a process called windowing in the time domain or apodization in the frequency domain. The time signal, Eq. 1, is multipled by a so-called window function prior to Fourier transformation. After Fourier transformation, the resultant "apodized" line shape has a much reduced skirt. Dozens of window functions have been described in the literature,[12] but little has been said about the criteria for choosing one particular window over others. Recently, we have proposed a "dynamic range criterion" for choosing which particular window function is most appropriate in a given experimental case. According to this criterion, the window function should be chosen to match the dynamic range of the spectrum. The dynamic range of the spectrum is the SNR of the largest peak or the ratio of the largest peak to the smallest peak of interest. The dynamic range of the window is approximately the ratio of the center peak to the largest auxiliary maximum.[11,13] Since each window function has its own dynamic range,[11] matching the window to the spectrum will give apodized spectra with the minimal line width, consistent with low spectral interference between peaks. We can recommend[11] the Hanning window for spectra with dynamic range <30, the Hamming window for spectra with 30 < dynamic range < 100, the Blackman-Harris window for spectra with 100 < dynamic range < 1000, and the Kaiser-Bessel window for spectra with 1000 < dynamic range. The set comprised of only these four windows is suitable for apodizing spectra which span over three decades of dynamic range. Accordingly, we have selected the line shapes corresponding to these four windows for examination in the present work.

The engineering literature[12] describes many windows and gives the corresponding apodized line shape when the window is applied to an *undamped* transient. As damped transients are common in chemical spectroscopy, we have derived the analytical form of the corresponding apodized line shape. The line shape for the Hanning-windowed (Eq. 28), damped transient was first given in Ref. 7. The analytical line shapes for the Hamming-windowed (Eq. 38) and the Blackman-Harris-windowed (Eq. 41) damped transients are first presented in this work.

Significance of Damping Ratio T/τ. In experimental practice, the time-domain signal, Eq. 1, can have any

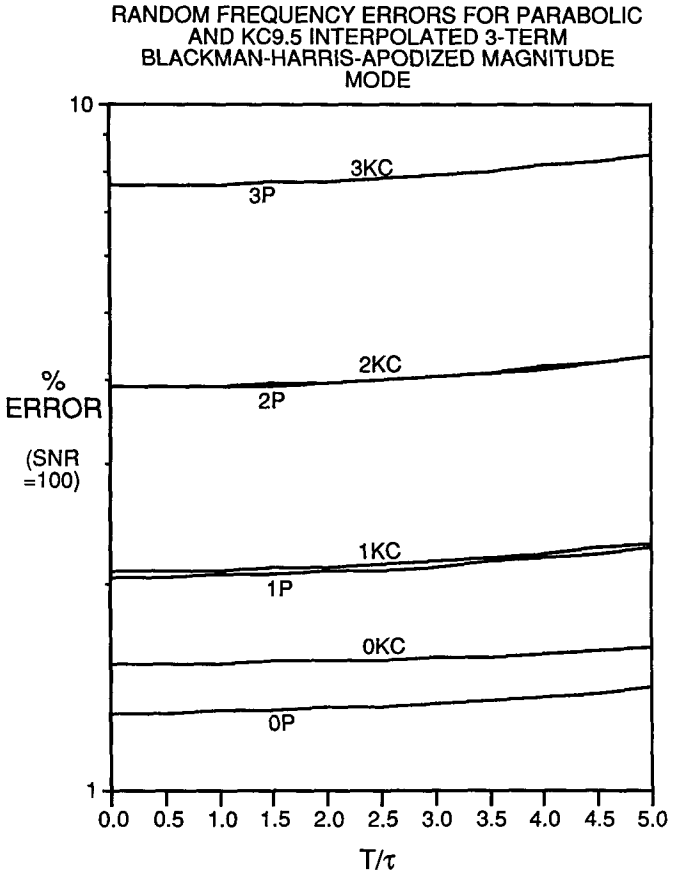

FIG. 8. Random frequency errors for parabolic (*P* curves) and *KC*9.5 (*KC* curves) interpolation of the zero-filled, Blackman-Harris-apodized, magnitude line shape as a function of T/τ. The errors are expressed as a percentage of the channel spacing in the non-zero-filled discrete spectrum (Eq. 3). The curves give the average random frequency error remaining after interpolation of the Blackman-Harris-apodized, zero-filled discrete line shape for which the noise level is 1% of the peak maximum (SNR = 100). For example, curve 2*KC* gives the average frequency error remaining after *KC*9.5 interpolation of the Blackman-Harris-apodized, twice-zero-filled discrete magnitude spectrum. Curve 0*P* gives the average frequency error remaining after parabolic interpolation of the Blackman-Harris-apodized, non-zero-filled, discrete magnitude spectrum. These error curves were calculated from Eqs. 22 and 46 with $e = 1$ for the *P* curves and $e = 6.6$ for the *KC* curves and then averaged according to Eqs. 25 and 26 as described in the text. The errors in this figure arise from the finite signal-to-noise ratio of the experimental data and should be added to the systematic errors given in Fig. 6 to predict the total error for a given experimental situation. The errors in this figure are proportional to the noise level (Eq. 24) and would be 10 times less for an SNR of 1000, 10 times greater for an SNR of 10, etc.

degree of damping, as characterized by the damping constant, T/τ. $T/\tau = 0$ describes an undamped transient; $T/\tau = 3.0$ describes a transient which has decayed to 5% of its initial value and is essentially completely damped. The present work, which allowed for $0 < T/\tau < 3$ for systematic errors and $0 < T/\tau < 5$ for random errors, thus essentially covers all possible cases from undamped to completely damped transients. While it is possible to use very long acquisition times to achieve large damping ratios, it is unproductive to do so, since past $T/\tau = 3$ there is virtually no signal left to acquire.

Since this damping ratio varies from spectrum to spectrum, and even from peak to peak within a given spectrum, we feel that any apodization/interpolation scheme

TABLE II. Maximum systematic frequency error (T/τ = 0-3.0)[a] for interpolation of apodized magnitude line shapes.

Interpolating scheme		Parabolic[b]	Magnitude Lorentzian[c]	*KCe*[d]
Window		%	%	%
Rectangle[e]	0[f]	23.397[g]	0.0[h]	17.842
	1	1.632[g]	5.430[h]	0.690
	2	0.183[g]	0.610[h]	0.066
	3	0.022[g]	0.073[h]	0.008
Hanning	0	5.281[g]	14.347[g]	0.342
	1	0.632[g]	1.745[g]	0.031
	2	0.078[g]	0.215[g]	0.004
	3	0.010[g]	0.027[g]	0.0005
Hamming	0	6.800[g]	16.774[g]	0.306
	1	0.811[g]	2.109[g]	0.027
	2	0.099[g]	0.261[g]	0.003
	3	0.012[g]	0.033[g]	0.0004
Blackman-Harris	0	4.560[g]	10.516[g]	0.041
	1	0.558[g]	1.320[g]	0.006
	2	0.069[g]	0.165[g]	0.0007
	3	0.008[g]	0.021[g]	0.0001

[a] Maximum systematic frequency error, for whatever value of T/τ and whatever value of ϕ that gave the largest error, expressed as a percentage of the channel spacing (Eq. 4) in the non-zero-filled discrete spectrum.
[b] From Eq. 21 (e = 1).
[c] From Eq. 21 (e = −½) or Eq. 36 of Ref. 4.
[d] From Eq. 21. The errors shown in the table are for whatever value of e that gave the best results for each window (Table I) except for the rectangle window for which e = 6.6.
[e] Unapodized line shape.
[f] Number of zero-fillings after windowing, prior to Fourier transformation.
[g] These cases have been previously examined[4] by numerical methods.
[h] These cases have been previously examined[3] by analytical methods.

should best operate independent of this ratio. We have previously shown that the dependence of apodization efficiency is essentially independent of T/τ (compare figs. 1 and 2 of Ref. 13). In this work we have examined the dependence of interpolation efficacy over the range of T/τ values which can occur in practice and have shown that this efficacy is esentially independent of T/τ (see Figs. 2, 4, and 6). As a consequence, one can recommend a particular windowing function on the basis of only the dynamic range of the spectrum[11] and can then chose from Table I the *KCe* interpolating function which minimizes the systematic interpolation error for that window.

Systematic Errors for *KC* Interpolation. The experimental Fourier method has a systematic error arising from the discrete nature of the experimental Fourier spectrum (see Figs. 1 and 7). This error can be minimized by zero-filling[2] and/or by interpolation. We have previously examined[4] the efficacy with which the parabola (Eq. 6), the Lorentzian function (Eq. 7), and the magnitude-Lorentzian (Eq. 8) interpolate towards the true location, ω_0, of the spectral peak. For apodized spectra, we found that the parabola is the interpolating function with the lowest residual error. Because the parabola is the best previously examined interpolation function,[4] we have compared the efficacy of *KCe* interpolation with that of parabolic interpolation in the present work.

The process called zero-filling involves increasing the length of the original discrete data set by adding a set of zeros at the end. Each additional zero-filling doubles the length of the "zero-filled time-domain data set." After Fourier transformation, the length of the discrete frequency spectrum is also doubled for each zero-filling, and the channel spacing in the discrete frequency spectrum is halved. Each additional level of zero-filling then provides an additional discrete intensity between each two adjacent discrete intensities.[1,2] For example, for Figs. 1 and 7, which show the discrete intensities in the non-zero-filled spectrum, one additional zero-filling would give an additional discrete intensity halfway between $m - 1$ and m and also halfway between m and $m + 1$. Since additional zero-filling gives a set of three discrete intensities which are closer to the continuous frequency, ω_0, than the set of three intensities in the less zero-filled spectrum, it is not surprising that zero-filling prior to interpolation reduces the residual systematic frequency error of three-point interpolation. This is true both for parabolic interpolation and *KCe* interpolation (see Figs. 2, 4, and 6). Examination of Figs. 2, 4, and 6 and Table II indicates that each additional level of zero-filling lowers the systematic error by about an order of magnitude. It should be noted, though, that the *random* error in the discrete magnitude *intensities* is not affected by zero-filling.[1]

For each of the three apodized line shapes discussed above, *KCe* interpolation gives a much better estimate of the true continuous frequency, ω_0, than does parabolic interpolation. A comparison of the residual systematic errors remaining after *KCe* interpolation with the corresponding errors remaining after parabolic interpolation is given in Table II. Table II lists the worst-case systematic error, for whatever value of ϕ (Eq. 10) and whatever value of T/τ that gave that error, for interpolation of discrete magnitude intensities. Also listed for comparison are the errors for interpolation of the "natural" (rectangle-apodized) line shape. For the Hanning-apodized line shape, *KC*5.5 interpolation of the non-zero-filled spectrum gives a worst-case residual error of 0.342% of the non-zero-filled channel spacing, which is fifteen times lower than the corresponding error for parabolic interpolation (5.281%). Similarly, *KC*6.6 interpolation of the Hamming apodized line shape of the non-zero-filled spectrum gives a worst-case residual error of 0.306% of the non-zero-filled channel spacing, which is twenty times lower than the corresponding error for parabolic interpolation (6.80%). The corresponding error for *KC*9.5 interpolation of the Blackman-Harris line shape is 0.041%, which is eighty times less that the corresponding error for parabolic interpolation (4.56%). In all cases then, *KCe* interpolation of the apodized line shape is significantly more accurate than parabolic interpolation, the best previously examined[4] interpolation scheme for apodized line shapes.

Random Errors for *KCe* Interpolation. In this work we wished to examine the total range of dampings from no damping to complete damping in order to cover all cases which could occur in experimental practice. A transient which has decayed to 5% of its initial value (T/τ = 3.0) is essentially completely damped and we have used T/τ = 3.0 as a practial upper limit for examining the systematic error in *KCe* interpolation (see Figs. 2, 4, and 6). When examining the random error, we noticed a slight but consistent increase in error with increasing damping and for this reason we extended the study of random

errors (Figs. 3, 5, and 8) to $T/\tau = 5.0$. As can be seen from these figures, no marked increases occur, as the behavior of the curves over the range $3.0 < T/\tau < 5.0$ can be predicted by extrapolation from the range $T/\tau < 3.0$.

A characteristic of the random error graphs (Figs. 3, 5, and 8) is that the random error depends little upon window function. This is evident from the curves in any one of these figures, which compare the random error of parabolic interpolation with that of *KCe* interpolation. It is also evident from comparisons among these figures, which show the random error for different *KCe* functions. For *KCe* interpolation of a non-zero-filled spectrum whose SNR = 100, the random frequency error is close to 1.5% of a channel spacing in all cases. It appears that, in general, the random error for three-point interpolation depends only slightly upon either window function or upon interpolation function.

As was the case for systematic errors, the random errors for *KCe* interpolation are essentially independent of the damping ratio T/τ (see Figs. 3, 5, and 8).

As mentioned above, zero-filling prior to interpolation *decreases* the residual *systematic* interpolation error (Figs. 2, 4, and 6 and Table II). On the other hand, additional zero-filling *increases* the residual *random* interpolation error (Figs. 3, 5, and 8). In all cases examined here (Figs. 3, 5, and 8), each additional level of zero-filling roughly doubles the random error. Zero-filling of a magnitude spectrum does not change the random uncertainties of the individual discrete spectral *intensities*.[1] Zero-filling just adds more discrete spectral intensities.[1] This increase in the random frequency error with greater zero-filling has also been noted for the exact interpolation of the unapodized magnitude line shape, Eq. 5.[14]

The increase in the random frequency error with greater zero-filling requires some explanation. The present work utilizes three-point fitting of a parabola (Eqs. 16 and A1–A3). Perhaps the most facile argument for explaining the increase in random frequency error with increasing zero-filling is with reference to the analogous case of two-point fitting of a linear function. Consider Fig. 9, which graphically describes the problem. Consider the case where a linear function, whose x-intercept is required, is to be fitted to two data points. Furthermore, assume that the x-axis error is negligible but the y-position has a random uncertainty. This would correspond to experimental Fourier spectroscopy where the frequency scale is well defined but the discrete amplitudes in the spectrum always have some random error. Consider, first, data set **A** (x_{A1}, y_{A1}; x_{A2}, y_{A2}), which has a random ordinate error Δy, for each data point. Either solid line in Fig. 9 fits data set **A**, and the x-axis intercepts of the two lines give rise to an uncertainty, Δx_A, in the x-axis intercept. Consider, next, data set **B** (x_{B1}, y_{B1}; x_{B2}, y_{B2}), where the abscissa spacing between the points of set **B** is less than the abscissa spacing for set **A**. The ordinate uncertainty, Δy, is the same for both data sets. Either dashed line in Fig. 9 fits data set **B**, and the x-axis intercepts of the two dashed lines give rise to an uncertainty, Δx_B, in the x-axis intercept. Note that the uncertainty of the x-axis intercepts for the dashed lines is *greater* than for data set **A**. The errors in the x-intercepts, ΔX_A and ΔX_B, are "two-point" errors, analogous to the "three-point" errors in the calculated frequency, ω_{interp}.

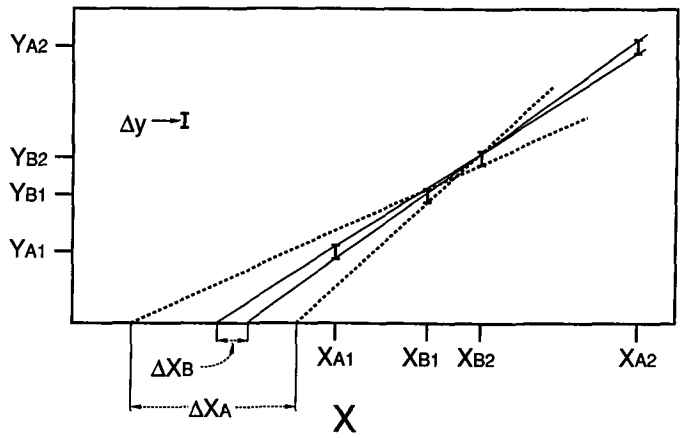

FIG. 9. Dependence of the random error in the calculated x-axis intercept, upon the x-axis spacing and the random uncertainty in the abscissa, Δy for two-point fitting of a linear function. The random ordinate error, Δy, is the same for both the **A** and the **B** data sets. The x-axis error is negligible for both data sets. Note that the uncertainty in the x-axis intercept, Δx, is much greater for data set **B**.

As mentioned above, the random errors are inherently inversely proportional to the SNR of the discrete spectral points. We have graphically presented the random errors for SNR = 100 in Figs. 3, 5, and 8, but the errors for any other SNR can be easily inferred from these figures.

Total Error for Parabolic Interpolation and *KCe* Interpolation. As mentioned earlier, parabolic interpolation is the best (i.e., it has the lowest systematic error) previously examined interpolation procedure for apodized magnitude line shapes.[4] The random errors for parabolic interpolation are given here (Figs. 3, 5, and 8) for the first time. Adding the systematic parabolic interpolation errors from the literature,[4] which are displayed in Figs. 2, 4, and 6, to the corresponding random errors in Figs. 3, 5, and 8, gives the total frequency error. Considering the dependence of the total frequency error of parabolic interpolation as a function of zero-filling leads to the following method for minimizing this total error: In all cases examined here, the minimum error results from parabolic interpolation of the *once*-zero-filled spectrum. These minimum total errors are, of course, greater than those of *KCe* interpolation.

Since a single zero-filling requires twice as much computer memory, a further advantage of *KCe* interpolation, compared with parabolic interpolation, over and above its greater accuracy, is that half as much computer memory is required. The fast Fourier transform times will also be less. Obviating the need for zero-filling is a major advantage of *KCe* interpolation.

***KCe* Interpolation and Exact Interpolation.** Recently, we have developed an interpolation method which *exactly* interpolates from the discrete intensities of an apodized Fourier spectrum to give the true continuous frequency, ω_0, the relaxation time, τ, and the scaling factor K (Eq. 1).[7] The methodology involves the simultaneous iterative solution of some fairly complex transcendental equations.[7,8] The iterative solution[15] of these equations requires as input an initial guess for ω_0, τ, and K. We found that parabolic interpolation gave an initial

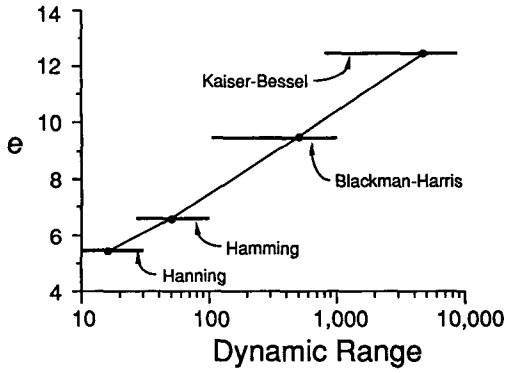

FIG. 10. Plot of optimal *KCe* exponent vs. dynamic range of the window. The horizontal bars indicate the span in dynamic range[11] over which the particular window is suitable. For each window, the solid circles are located at half of the maximum of the span in dynamic range. The *KCe* values for the Hanning, Hamming, and Blackman-Harris windows are taken from Table I. The *KCe* exponent value of $e = 12.5$ for the Kaiser-Bessel window is estimated from this figure.

guess for ω_0 that lead to fairly rapid iteration to the exact value for ω_0.[7] Subsequently,[8] we have used *KCe* interpolation to calculate the initial guess for ω_0 and we find that it gives more rapid convergence to the true value for ω_0 than does parabolic interpolation. In addition, the input guess for ω_0 from *KCe* interpolation makes the iterative solution less sensitive to the initial guesses of the other input variables.

Estimated *KCe* Function for the Kaiser-Bessel Line Shape. One of the windows which we have found suitable for wide-dynamic-range spectra is the Kaiser-Bessel window. We have recommended[11] this window for spectra whose dynamic range spans 1000:1 to 10,000:1. The analytical form of this window prevents easy derivation of its magnitude spectrum and the associated rigorous determination of its optimal *KCe* exponent. Nevertheless, we can estimate an optimal *KCe* exponent by extrapolation from the other optimal *KCe* exponents mentioned above. Figure 10 shows a plot of the dynamic range vs. *KCe* exponent for various windows. The span in dynamic range for each of the windows is indicated by a "spanning line" and is 10:1 to 30:1 for the Hamming window, 20:1 to 100:1 for the Hamming window, 100:1 to 1000:1 for the Blackman-Harris window, and 1000:1 to 10,000:1 for the Kaiser-Bessel window. The solid circles are located at half the maximum dynamic range for each of the first three windows: 15:1 for the Hanning window, 50:1 for the Hamming window, and 500:1 for the Blackman-Harris window. If we wish to locate the corresponding midpoint (5000:1) of the Kaiser-Bessel window by extrapolation of the midpoints of the other windows, then the Kaiser-Bessel "spanning line" has to be located at $e = 12.5$. In this manner we estimate the optimal *KCe* exponent for interpolation of the Kaiser-Bessel line shape to be $e = 12.5$.

The physical basis for the legitimacy of the extrapolation in Fig. 10 is the change in line shape as one progresses to line shapes of greater dynamic range and the corresponding change in the shape of the *KCe* function as e increases. Line shapes of greater dynamic range have "flatter tops," "broader middles," and "steeper sides" than line shapes of lesser dynamic range (see figs. 1 and 2 of Ref. 13). These changes are mimicked by the *KCe* function as the exponent e increases.

TABLE III. Recommended windows and *KCe* functions.

Dynamic range of spectrum	Recommended window[a]	*KCe* exponent, e
5–30	Hanning	5.5[b]
30–100	Hamming	6.6[b]
100–1000	Blackman-Harris	9.5[b]
1000–10,000	Kaiser-Bessel	12.5[c]

[a] From Ref. 11.
[b] From Table I.
[c] From Fig. 10.

As noted above, the random errors for *KCe* interpolation depend upon the number of zero-fillings but are esentially independent of the apodizing window and of the particular *KCe* function. This is particularly true for *KCe* interpolation of the non-zero-filled spectrum where the random frequency error for SNR = 100 is about 1.5% in all cases (Figs. 3, 5, and 8). Accordingly, we estimate that the random errors for *KC*12.5 interpolation of the Kaiser-Bessel line shape are about the same as those in Figs. 3, 5, and 8.

Experimental Application of *KCe* Interpolation. The interpolated frequencies, derived in the prior sections, were derived with a knowledge of the analytical form of the magnitude line shapes. In experimental practice, however, ω_{interp} has to be calculated from the experimental variables of the experiment. In experimental practice then, *KCe* interpolation of the discrete magnitude intensities is given by Eq. 47, rather than Eq. 20:

$$\omega_{\text{interp}} = \frac{2\pi m S}{2^n N} - \frac{\pi S}{2^n N} \times \left[\frac{[C(m+1)]^{1/e} - [C(m-1)]^{1/e}}{[C(m-1)]^{1/e} - 2[C(m)]^{1/e} + [C(m+1)]^{1/e}} \right]. \quad (47)$$

Equation 47 gives ω_{interp}, the interpolated peak frequency, as a function of S, the sampling rate; N, the number of data points in the non-zero-filled time signal; n, the number of zero-fillings; m, the index value of the discrete local maximum; $C(m)$, the local maximum; and $C(m-1)$ and $C(m+1)$, the discrete intensities on either side of $C(m)$.

Examination of Table I shows that, while a particular value for the *KCe* exponent is optimal, the error trend in the neighborhood of the optimal *KCe* exponent is broad minimum. For example, for the Blackman-Harris line shape, *KC*9.5, the optimal *KCe* function, gives a residual systematic error of 0.041% of a channel spacing. On the other hand, *KC*8.0 gives an error only three times greater (0.137%), which is still much less than the random error for SNR = 100 and about the magnitude of the random error for SNR = 1000 (Fig. 6). For the Hanning-apodized line shape, *KC*4.0 (0.754% error) is close in efficacy to the optimal *KC*5.5 (0.342% error) function. For the Hamming-apodized line shape, *KC*8.0 (0.532% error) is close to the optimal *KC*6.6 (0.306% error) function. Use of close-to-optimal values of e may, in exper-

imental practice, be desirable for the following reason: Calculation of roots with a digital computer involves three steps—calculation of the logarithm by power series expansion, division of the log by the root, and exponentiation by power series expansion. The middle step, division by the root, is much faster for roots which are powers of two. These divisions can be accomplished by machine language shift operations rather than by calls to the arithmetic logic unit (ALU). Division calls to the ALU are among the slowest operations for digital computers. Avoiding these calls by using shift operations with power-of-two roots may justify use of these roots. Similarly, using a single, special power series for a specific root may be worth considering if this power series converges rapidly.

RECOMMENDATIONS

Combining our prior work on selection[11] of optimal apodizing windows with the present work on optimal interpolation functions allows recommendations to be made for many experimental situations. The dynamic range of the spectrum determines the optimal window, and the optimal *KCe* function then follows from Table I and Fig. 10. These recommendations are summarized in Table III. In all cases, these recommended apodization/interpolation schemes should be applied to the *non*-zero-filled spectrum, as use of the non-zero-filled magnitude intensities will give the lowest overall frequency error. For situations in which parabolic interpolation is used, the minimum total error, which will be larger than that from *KCe* interpolation, follows from interpolation of the once-zero-filled spectrum.

ACKNOWLEDGMENTS

This research was supported by the Natural Sciences and Engineering Research Council of Canada. The authors would like to thank Pat Tang for many helpful discussions of this work.

1. E. Bartholdi and R. E. Ernst, J. Mag. Reson. **11,** 9 (1973).
2. M. B. Comisarow and J. Melka, Anal. Chem. **51,** 2198 (1979).
3. C. Giancaspro and M. B. Comisarow, Appl. Spectrosc. **37,** 153 (1983).
4. A. Serreqi and M. B. Comisarow, Appl. Spectrosc. **41,** 288 (1987).
5. A. G. Marshall, M. B. Comisarow, and G. Parisod, J. Chem. Phys. **71,** 4434 (1979).
6. K. H. Chow and M. B. Comisarow, Comput. Chem. **13,** 291 (1989).
7. C. D. Keefe and M. B. Comisarow, Appl. Spectrosc. **43,** 605 (1989).
8. C. D. Keefe and M. B. Comisarow, paper in preparation.
9. F. B. Hildebrand, *Introduction to Numerical Analysis* (McGraw Hill, New York, 1974), p. 75.
10. B. A. Barry, *Errors in Practical Measurement in Science, Engineering, and Technology* (John Wiley and Sons, New York, 1978), pp. 72–78.
11. J. P. Lee and M. B. Comisarow, Appl. Spectrosc. **41,** 93 (1987).
12. F. J. Harris, Proc. I. E. E. E. **66,** 51 (1978).
13. M. Aarstol and M. B. Comisarow, Int. J. Mass Spec. Ion Proc. **76,** 287 (1987).
14. F. R. Verdun, C. Giancaspro, and A. G. Marshall, Appl. Spectros. **42,** 715 (1988).
15. D. B. Dulley and M. L. V. Pitteway, Commun. ACM **10,** 726 (1967).

APPENDIX

This work was concerned with interpolation from the discrete Fourier spectrum to give, via Eq. 20, the interpolated frequency, ω_{interp}, of the continuous spectrum. This process does not require that the coeffcients a, b, and c in the interpolating function, Eq. 9, be known. These coefficients *are* needed, though, for *plotting* the interpolating function, as is done in Figs. 1 and 7. The expressions for the coefficients a, b, and c, in terms of the intensities, $C(\omega_m)$, and the frequencies, ω_m, are given by Eqs. A1–A3.

$$a = \frac{C(\omega_m)^{1/e} - C(\omega_{m+1})^{1/e} - b(\omega_m - \omega_{m+1})}{(\omega_m^2 - \omega_{m+1}^2)} \tag{A1}$$

$$b = \frac{C(\omega_{m-1})^{1/e} - C(\omega_m)^{1/e} - \left[\dfrac{[C(\omega_m)^{1/e} - C(\omega_{m+1})^{1/e}](\omega_{m-1}^2 - \omega_m^2)}{(\omega_m^2 - \omega_{m+1}^2)}\right]}{\omega_{m-1} - \omega_m - \left[\dfrac{(\omega_{m-1}^2 - \omega_m^2)(\omega_m - \omega_{m+1})}{(\omega_m^2 - \omega_{m+1}^2)}\right]} \tag{A2}$$

$$c = C(\omega_{m-1})^{1/e} - a\omega_{m-1}^2 - b\omega_{m-1} \tag{A3}$$